Effect of pH on Synthesis and Properties of Perovskite Oxide via a Citrate Process

Zhentao Wu, Wei Zhou, Wanqin Jin, and Nanping Xu
Membrane Science and Technology Research Center, Nanjing University of Technology, Xinmofan Road 5, Nanjing 210009, People's Republic of China

DOI 10.1002/aic.10664
Published online September 16, 2005 in Wiley InterScience (www.interscience.wiley.com).

A series of $La_{0.6}Sr_{0.4}Co_{0.4}Fe_{0.6}O_{3-\delta}$ (LSCF) perovskite-type oxides were synthesized using a modified citrate process under various pH conditions (pH =1, 3, 5, 7, and 9, respectively). The effect of pH on the chelate process, crystal development, morphology, and oxygen permeability of LSCF oxides were investigated. FT-IR analysis showed that the chelate processes for pH = 1 and 3 were different from those for pH = 5, 7, and 9. XRD and SEM observations revealed that the crystal formation and morphology of LSCF oxides were dependent on the precursors with different pH conditions. The LSCF membranes derived from the precursors with lower pH values (pH = 1 and 3) exhibited larger apparent activation energy for oxygen permeation than the other samples (pH = 5, 7, and 9) in the range of 1073-1123K. This study indicated that properties such as crystallinity and oxygen permeability of LSCF oxide could be tailored by controlling the pH values in the synthesis process. © 2005 American Institute of Chemical Engineers *AIChE J,* 52: 769–776, 2006

Keywords: pH, perovskite-type oxides, synthesis, citrate process, oxygen permeability

Introduction

Mixed ionic-electronic conducting oxides (MIECOs) are one kind of material exhibiting both high oxygen ionic and electronic conductivity simultaneously at high temperatures, typically above 973K.[1] The main advantages of such materials are related to an infinite theoretical permselectivity with respect to oxygen, caused by the only possible mechanism of oxygen transport, that is, oxygen ion hopping between neighboring vacant sites in the crystal lattice. Considerable attention has been attracted by these materials as possible candidates applied in oxygen separation,[1-7] solid oxide fuel cells,[8-11] and membrane reactors.[12-19]

Factors (such as the preparation methods,[20-24] the sintering profile,[25,26] the hydrolysis rates,[27] and the membrane shaping process[28]) that affect the properties of MIECOs and the corresponding membranes have been extensively studied when researchers made great efforts to figure out the relationships between the materials' structures and the synthesis processes. As for the synthesis methods, wet chemical ways are always favored because the materials synthesized in these ways can be of accurate stoichiometric components and free of impurities. The properties of the materials prepared by wet chemical routes are highly dependent on the kind and the nature of the chemical species in the precursors, and the chemical species are always significantly influenced by many variables, such as pH, temperature, concentration, and so on. Among these, the pH condition is often considered as one of the most important factors. Alejandro[29] synthesized Silica-HAp composites of different particle shapes and sizes (from several nanometers to microns) by controlling the pH value from 5 to 9. Tsai et al.[5] produced different compositions of perovskite oxides under basic (pH = 9) conditions. Xie et al.[30] prepared nanoscaled $BaBi_4Ti_4O_{15}$ (BBT) powder with homogenous particle size using the sol-gel method, in which the BBT precursor was stable when the pH value was at 3.5.

The modified citrate process,[31] which was originally developed by Pechini to prepare capacitor oxides in the 1960s,[32] has

Correspondence concerning this article should be addressed to N. Xu at npxu@njuct.edu.cn.

been employed to synthesize complex oxides. In the synthesis process, citric acid prefers to chelate with various cations in the precursors by forming a polybasic acid. The chelate complexes undergo polyesterification when heated in the presence of polyhydroxyl alcohol (usually ethylene glycol) and form a rigid resin intermediate. The organic substances in the resin intermediate decompose and are burned off during firing, which provides additional combustion heat for the calcination. It is noted that the weak triprotic citric acid with chemical formula of $C_6H_8O_7$ (H_3L) dissociates in a stepwise way in the solutions depending on the pH values as follows:[33]

$$H_3L = H^+ + H_2L^- \quad \log K_1 = -3.10 \tag{1}$$

$$H_2L^- = H^+ + HL^{2-} \quad \log K_2 = -4.80 \tag{2}$$

$$HL^{2-} = H^+ + L^{3-} \quad \log K_3 = -6.40 \tag{3}$$

where K_i is the corresponding ionization equilibrium constant.

Although the modified citrate route has been frequently applied in preparing perovskite-type and perovskite-related oxides,[5,23,34,35] few studies focused on the effects of pH on the synthesis process and the properties of these oxides. The objectives of this study, therefore, were mainly to investigate the effects of pH on the material properties, such as the crystal development and the oxygen permeability of perovskite-type oxides. $La_{0.6}Sr_{0.4}Co_{0.4}Fe_{0.6}O_{3-\delta}$ (LSCF) was selected in this study because it belongs to the families of $La_{1-x}A_xCo_{1-y}Fe_yO_{3-\delta}$ (A = Sr, Ba, Ca) ($0 \le x \le 1$, $0 \le y \le 1$) perovskite-type oxides that have been extensively studied for oxygen permeation.[3,5,36,37]

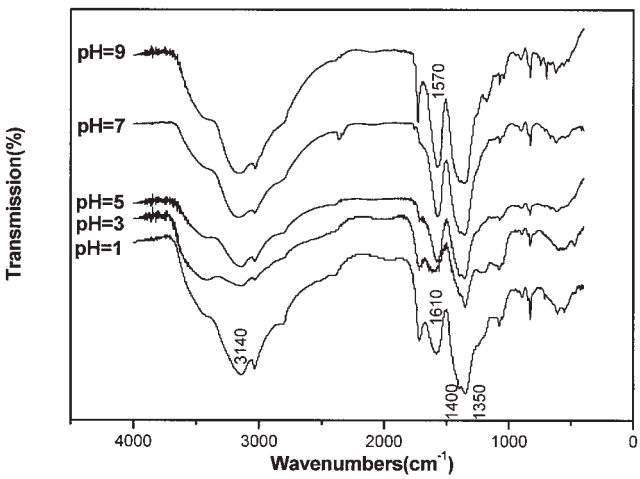

Figure 1. FT-IR images of various pH-valued precursors. The bands at about 3140 and 1350 cm^{-1} correspond to the O-H group of citric acid and asymmetric NO_3^- vibration, respectively.

Asymmetric stretching vibrations $\nu_{as}(COO^-)$ appear between 1610 and 1570 cm^{-1}, whereas the symmetric ones $\nu_s(COO^-)$ appear at about 1400 cm^{-1}.

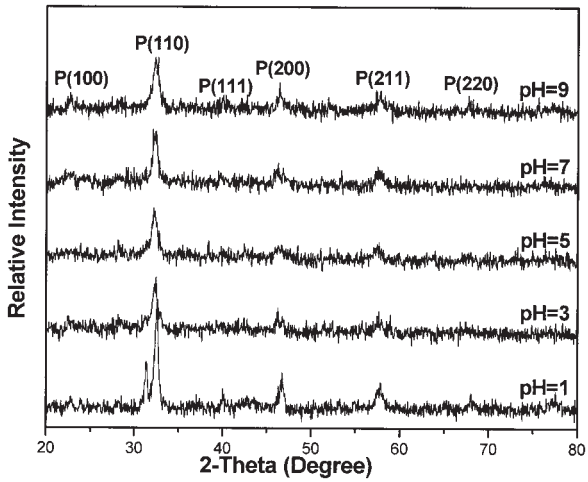

Figure 2. XRD patterns of the primary powders originating from various pH-valued precursors.

Experimental

Sample synthesis

Analytical grade $La(NO_3)_3{\cdot}6H_2O$, $Sr(NO_3)_2$, $Co(NO_3)_2{\cdot}6H_2O$, and $Fe(NO_3)_3{\cdot}9H_2O$ were used as the starting materials to synthesize LSCF precursors. Stoichiometric amounts of nitrates were dissolved into a certain volume of HNO_3 under agitation, and citric acid was then added at a ratio, citric acid to metal ions, of 2:1 at room temperature. The precursor was divided into five parts, which were adjusted to the pH values of 1, 3, 5, 7, and 9, respectively, by adding $NH_3{\cdot}6H_2O$(30%). All the precursors were then stirred continuously for 12 h at room temperature.

The primary powders were formed when the spontaneous combustion, which was triggered by the burning of the ammonium nitrate (NH_4NO_3), occurred when the precursors were dried at 453K. Then these pre-powders were grinded and calcined at various temperatures (873, 973, 1073, 1173, and 1223 K) for 5 h, respectively, in air with the heating and cooling rate of 2 $K{\cdot}min^{-1}$.

The powders calcined at 1223 K were uniaxially pressed at 300 MPa for 5 min to prepare the green disc membranes with the diameter of 16mm, which were free of the additives. The membranes were obtained after these green discs were sintered at 1473 K for 5 h in air with a heating and cooling rate of 2 $K{\cdot}min^{-1}$.

Characterization

Fourier transform infrared spectroscopy (FT-IR, Thermo Nicolet Corporation AVATAR-360) of the precursor was recorded from 4000-400cm^{-1} by the KBr pellet method. The precursors were dried at 60°C under vacuum for about 5 h to remove water before the analysis. The crystal structures of synthesized powders were determined by X-ray diffraction (XRD, Bruker D8 Advance) using CuKα radiation. The experimental diffraction patterns were collected at room temperature by step scanning in the range of $20° \le 0 \le 80°$ with 0.02° increments for calculating the lattice parameters or with 0.05° increments for the sinterability and crystal development. Scanning electron microscopy (SEM, JEOL-6300) was used to

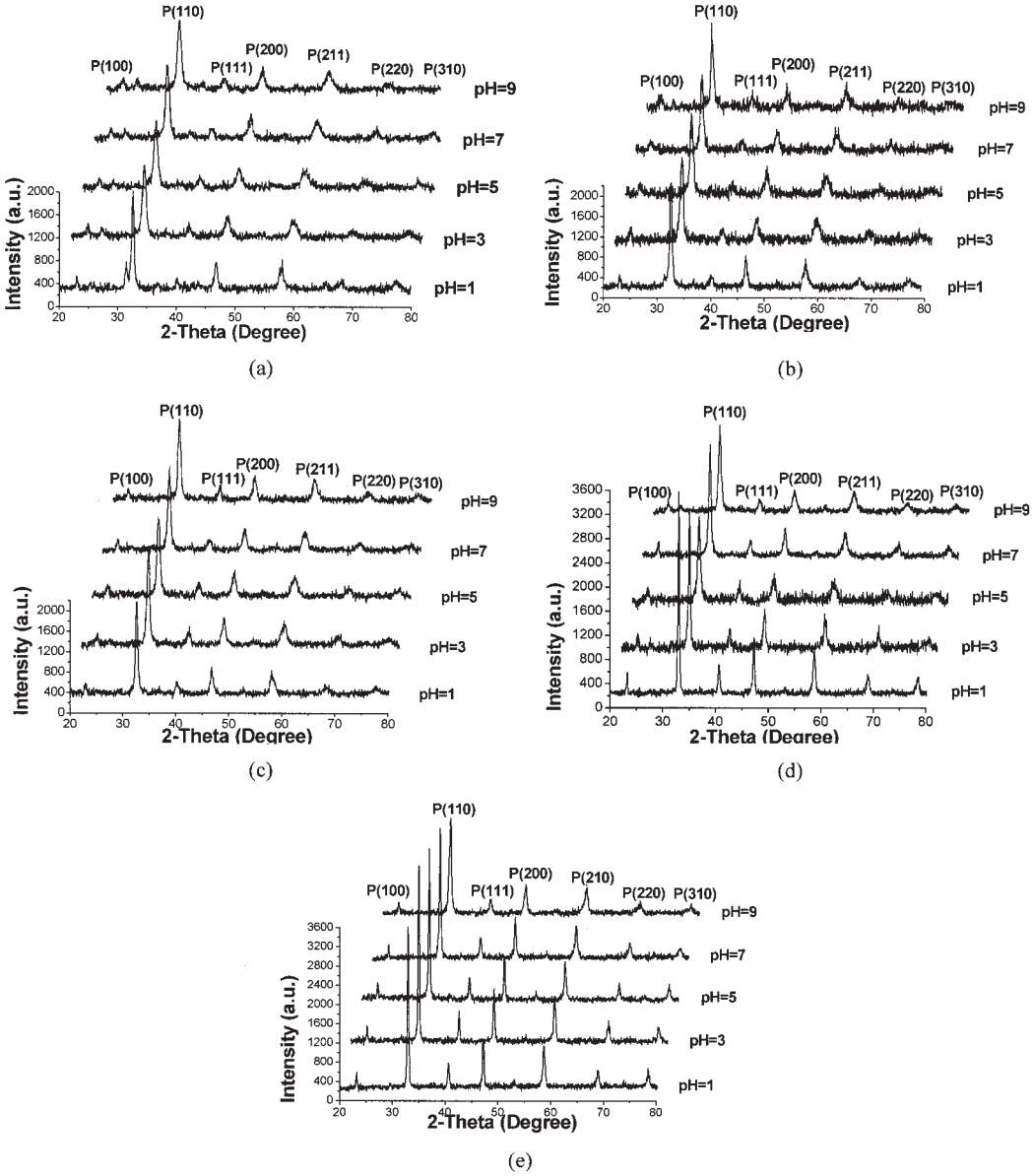

Figure 3. XRD patterns of LSCF powders calcined at (a) 873K, (b) 973K, (c) 1073K, (d) 1173K, and (e) 1223K with the same dwell time of 5 h.

observe the morphologies of the primary powders and the powders calcined at 1073 K. The morphologies of the LSCF membranes were observed using Environmental Scanning Electron Microscopy (ESEM, QUANTA-2000).

Oxygen permeation measurement was performed on the high temperature oxygen permeation apparatus in our laboratory, which was described elsewhere.[38] Disk membranes were polished to the same thickness of 1.1mm and sealed between two gold rings. The effective area for oxygen permeation was about 0.283cm^2. Before starting the oxygen permeation measurement, the assembly was heated from room temperature to 1313 K at a rate of 2 K·min^{-1} and held for 4 h to form the bonding. The temperature of interest was then controlled through adjusting the cooling rate (2 K·min^{-1}). One side of the membrane was exposed to air (P_{O2} = 0.209atm) at a flow rate of 100mL·min^{-1}, while the other side was exposed to a lower P_{O2} that was controlled by regulating the He flow rate by mass flow controllers (model D07/ZM, Beijing Jianzhong Machine Factory, China). A gas chromatograph (GC, Shimabzu model GC-7A) equipped with a 5A molecule sieve column was connected to the exit of the sweep side. The amount of oxygen passing through the membrane was calculated using the measured outlet flow rate and the oxygen content.

In order to simplify the narration, some symbols were used to designate the samples at different preparation and characterization stages. For example, the precursor with the pH value of A (A = 1,3,5,7,9) during the titration process (the stage of adjusting the pH values of the precursors) was designated as sample pHA$_a$, the primary powder derived from the sample pHA$_a$ was designated as sample pHA$_b$, the calcined powder

Table 1. Bandwidths at Half-Height ($P(110)$) at Various Temperatures and Lattice Parameters of LSCF Oxides Calcined at 1223 K for 5 h

pH Value	Bandwidths at Half-Height ($P(110)$)			Lattice Parameter (Å)	Unit Cell Volume (Å^3)	Crystal Structure
	1073 K	1173 K	1223 K			
1	0.497	0.297	0.266	3.853	57.19	Cubic
3	0.580	0.323	0.277	3.860	57.50	Cubic
5	0.728	0.597	0.283	3.863	57.63	Cubic
7	0.617	0.472	0.269	3.859	57.47	Cubic
9	0.637	0.558	0.254	3.855	57.28	Cubic

from sample pHA_b was named as sample pHA_c and the corresponding membrane was noted as sample pHA_d.

Results And Discussion

pH effect on the chelate process

In the first titration stage, the appearances of the precursors were found to change with the pH values: samples $pH1_a$ and $pH3_a$ were clear claret solutions, while yellow (sample $pH5_a$) or dark yellow (sample $pH7_a$) precipitates formed in a few hours after the pH value was adjusted to 5 or 7. The precursor turned into a clear dark claret solution again when more ammonia was added (sample $pH9_a$). XRD patterns of the precursors proved that no metal hydroxides formed even for the precursors with precipitates, which suggested that the variation of the appearances of the precursors were related with the different chelate processes that depended on the pH conditions. Figure 1 shows the FT-IR images of various pH-valued precursors. The bands at about 3140 and 1350cm^{-1} correspond to the O-H group of citric acid and asymmetric NO_3^- vibration, respectively. Asymmetric stretching vibrations $\nu_{as}(COO^-)$ appear at about 1610 or 1570 cm^{-1}, whereas the symmetric ones $\nu_s(COO^-)$ appear at about 1400cm^{-1}. All of the carbonyl absorptions are shifted to lower frequencies with respect to citric acid, which indicates a change in the vibrational status of the citrate anion upon coordination to the metal ions.[39-41] The asymmetric stretching vibrations $\nu_{as}(COO^-)$ appear at 1610 cm^{-1} for the samples with low pH values (samples $pH1_a$ and $pH3_a$), while they are at about 1570 cm^{-1} for the others (samples $pH5_a$, $pH7_a$, and $pH9_a$), which reflect different chelate processes between the citrate species and the metal species. With increase of the pH values, the citric acid dissociated more completely and more complex ligands of the citrate species participated in the chelate processes, which influenced the interactions among the metal species at the same time.

pH effect on the sinterability and crystal development of LSCF

Figure 2 shows the XRD patterns of the primary powders derived from various pH-valued precursors. Immature perovskite structure (except sample $pH1_b$) began to form during the spontaneous combustion when the precursors were heated to 453 K. Similar intensities of the characteristic peaks were observed for these primary powders, which should be ascribed to the lower combustion temperature (about 700-800 K). For sample $pH1_b$, a transient phase (from the precursor to the immature perovskite structure) forms. This is not only due to the insufficient combustion temperature resulting from the lesser amount of NH_4NO_3, but also to the probability of forming clusters of metal ions,[35] which is closely related with the interactions among the metal species in the precursors. This transient phase changed into perovskite structure when the calcining temperature was higher than 973K (Figure 3 b) because of the further solid-state reaction.

The primary powders were then calcined at 873, 973, 1073, 1173, and 1223K, respectively, for 5 h in order to investigate the sinterability and crystal development of the derived LSCF oxides. Figure 3 shows the XRD patterns of LSCF oxides calcined at different temperatures. Similar XRD patterns were observed below the calcining temperature of 1073K (Figures 3a-c). The intensities of the characteristic peaks of samples $pH1_c$ and $pH3_c$ were much larger than the other samples at 1173K and increased slowly from 1173 to 1223 K (Figures 3d and e), while the intensities of the characteristic peaks of samples $pH5_c$, $pH7_c$, and $pH9_c$ increased obviously from 1073 to 1223K (Figures 3d and e). All the samples calcined at 1223 K were fully developed into the cubic perovskite structure.

Based on the XRD patterns, the bandwidths at half-height (P(110)) and lattice parameters (calcined at 1223 K for 5 h) of LSCF oxides were calculated, as listed in Table 1. When the calcining temperature increased from 1073 K to 1173 K, the bandwidths at half-height (P(110)) of samples $pH1_c$ and $pH3_c$ decreased much faster than the others and changed little when the calcining temperature reached 1223 K. This indicated that the full perovskite structure of LSCF could form at a relatively lower calcining temperature or a shorter dwell time. For the samples derived from precursors with pH values of 5, 7, and 9, the bandwidths at half-height (P(110)) decreased with increasing the temperature from 1073 to 1223K, which indicated that the grain sizes grew with increase of temperature according to the Scherrer formula. All the samples calcined at 1223 K were of cubic perovskite structure, but the corresponding lattice parameters were different and in the order of sample $pH1_c <$ sample $pH3_c <$ sample $pH5_c >$ sample $pH7_c >$ sample $pH9_c$. This is consistent with the effects of pH on the chelate processes and suggests that the sinterability and crystal development of LSCF oxides derived from the precursors with pH values of 1 and 3 are different from the other samples.

pH effect on the morphologies of LSCF powders and membranes

Figure 4 shows the SEM images of the morphologies of LSCF primary powders and those calcined at 1073 K for 5 h, respectively. The temperature of 1073 K was chosen as the calcining temperature in order to avoid serious aggregation.[35] The LSCF samples derived from the precursors with pH values of 3, 7, and 9 were chosen to observe the trend of the pH effects on the powder morphologies. As shown in Figure 4, the particle

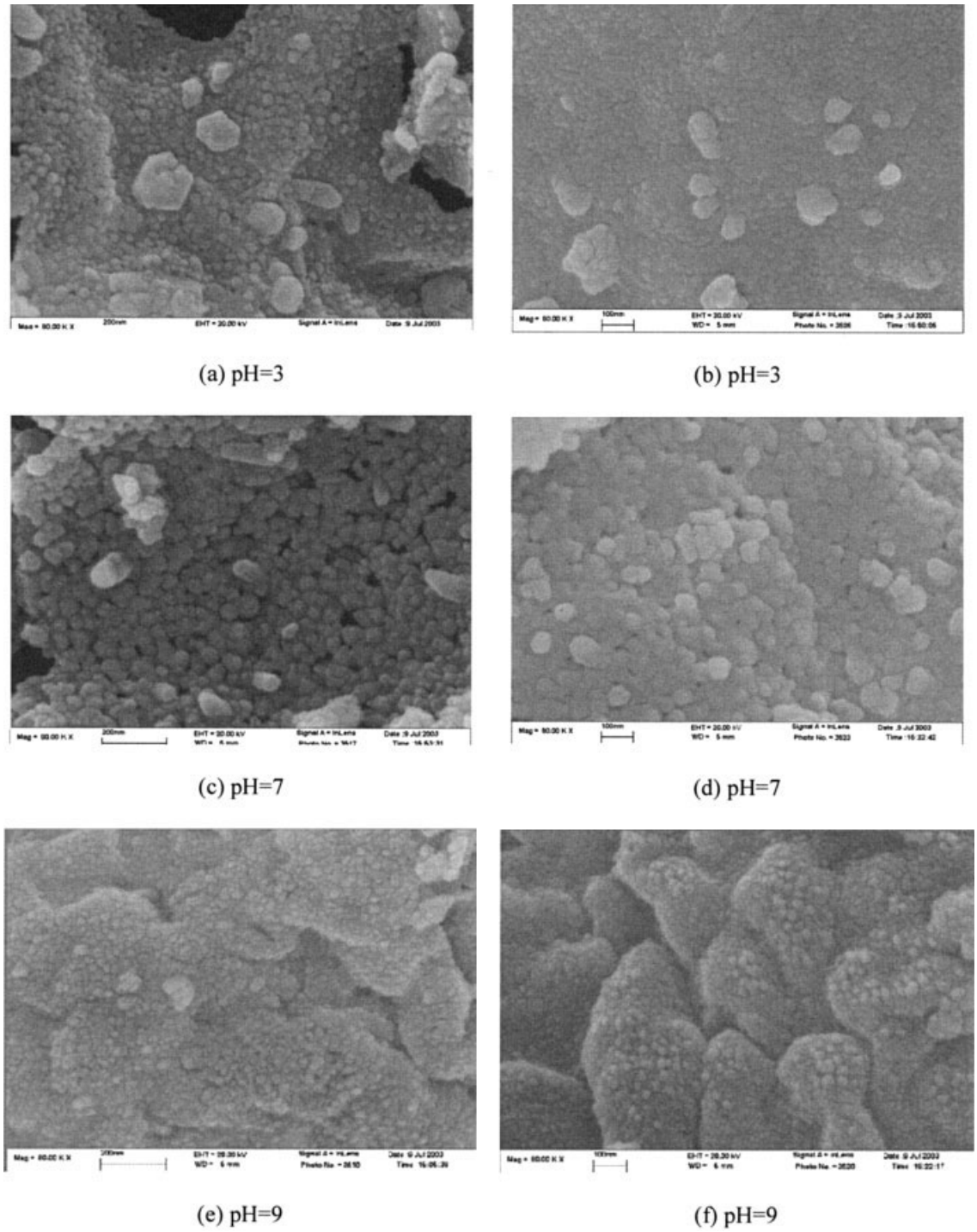

Figure 4. SEM images of the morphologies of LSCF primary powders (a), (c), and (e), and those calcined at 1073 K for 5 h (b), (d), and (f).

shapes were almost independent of the pH conditions. But the change of the average particle sizes (both the primary powders and the calcined ones) was similar to that of the corresponding lattice parameters.

Morphologies of the cross-sections of the membranes derived from the different pH-valued precursors are presented in Figure 5. For the membranes originated from the low pH-valued precursors (pH = 1 and 3), no obvious grain boundaries are observed except at the edges of some voids (Figures 5a and b). Clear grain boundaries and polyhedral grains appeared (Figure 5c and d) for the membranes from the precursors with pH value of 5 and 7. For sample $pH9_d$, although some grains fused together to some extent, the grains boundaries could still be observed (Figure 5e). The dependencies of the microstructures of the LSCF membranes on pH conditions agree well with all the phenomena observed above.

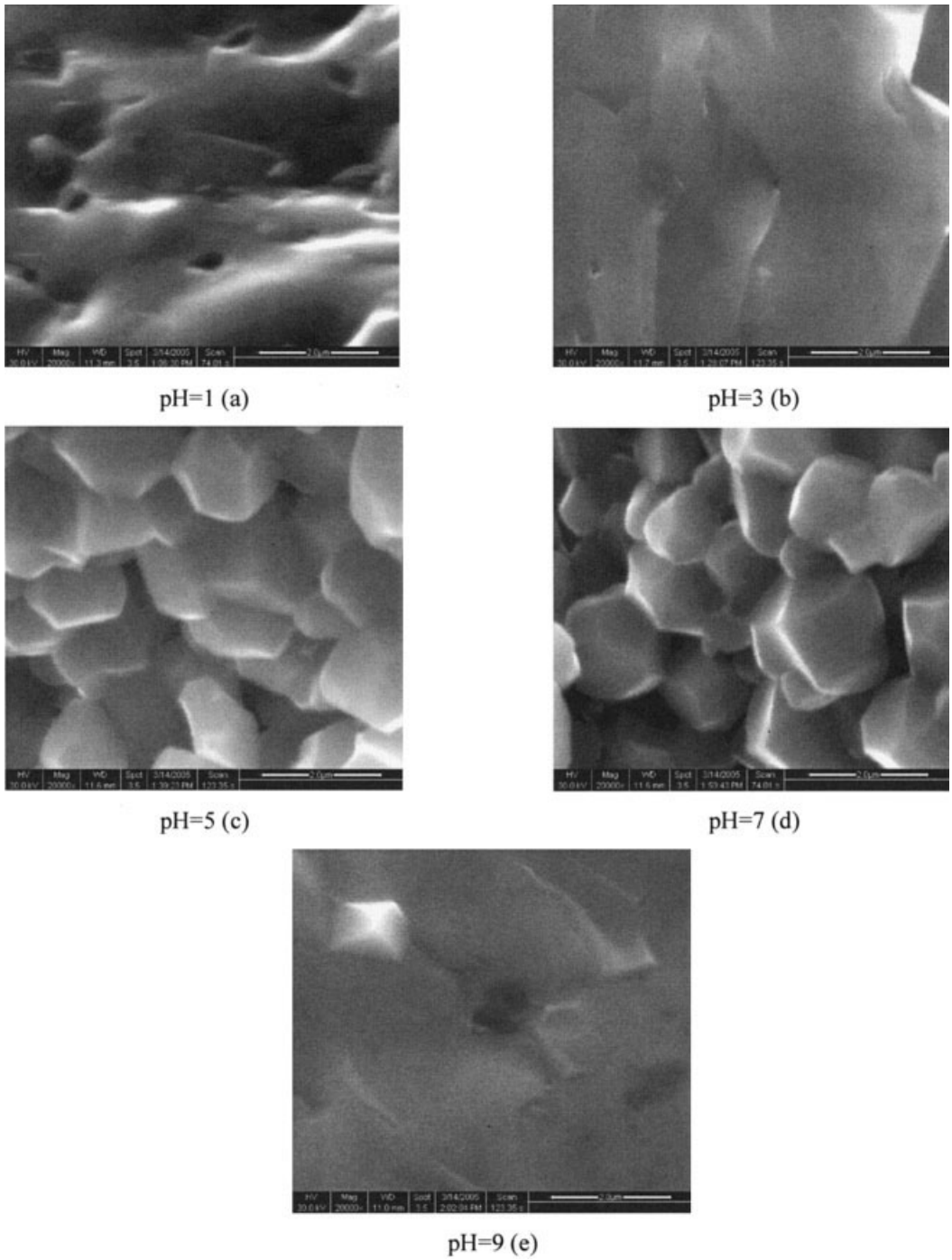

Figure 5. ESEM images of the cross-sections of the LSCF membranes derived from the precursors with various pH values.

(a) pH = 1, (b) pH = 3, (c) pH = 5, (d) pH = 7, and (e) pH = 9.

pH effects on the oxygen permeability of LSCF

The temperature dependence of oxygen permeation fluxes through LSCF membranes is shown in Figure 6. All samples were measured at identical experimental conditions. The measurements were conducted in the range of 1073-1123K. As shown, the oxygen fluxes decreased monotonically with decreasing the temperature. Oxygen fluxes of samples $pH1_d$ and $pH3_d$ were found to be more sensitive to the temperatures than the other samples (samples $pH5_d$, $pH7_d$, and $pH9_d$). The corresponding apparent activation energies (Ea) of oxygen permeation for samples $pH1_d$ and $pH3_d$ were 134.77 and 164.06 kJ/mol, respectively, which are significantly larger than the other samples (Ea = 76.57, 82.32, and 98.21 kJ/mol for samples $pH5_d$, $pH7_d$, and $pH9_d$, respectively). This is due to the pH-dependent microstructures of the LSCF membranes (Figure 5). Generally, the Ea values are greatly influenced by the

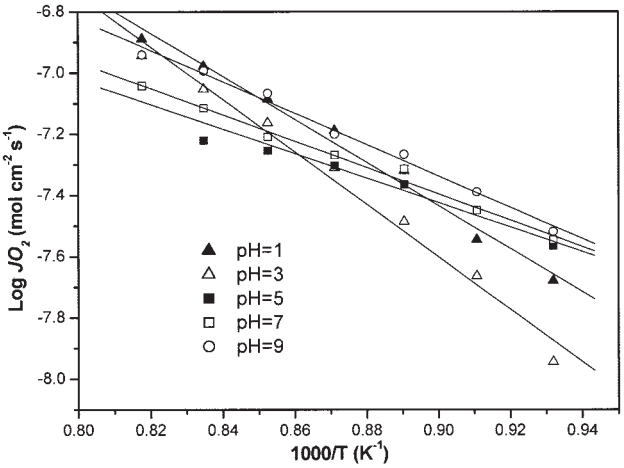

Figure 6. Temperature dependence of oxygen permeation fluxes through the membranes of samples $pH1_d$, $pH3_d$, $pH5_d$, $pH7_d$, and $pH9_d$; the sintered membrane disc was placed in air/helium at the oxygen partial pressure gradient of $0.21/1 \times 10^{-3}$ atm.

average bound energy (ABE), the free volume (V_F), the properties of the grain, and grain boundaries.[42] Oxygen ions transport in the dense ceramic membrane by hopping between neighboring vacant sites in the crystal lattice, in which the oxygen ions must squeeze past the surrounding atoms at the expense of energy (Ea). But, at the grain boundaries, along which atoms are not as orderly placed as they are in the grains, oxygen ions need less energy to transport. As shown in Figure 5, samples $pH1_d$ and $pH3_d$ exhibited microstructures with few obvious grain boundaries, which resulted in much larger Ea values. Similarly, the smaller Ea values of the samples $pH5_d$, $pH7_d$, and $pH9_d$ resulted from the obvious grain boundaries in the microstructures. The order of Ea values for samples $pH5_d$, $pH7_d$, and $pH9_d$ corresponds to the order of lattice parameters.

Conclusions

The effect of pH condition on properties of LSCF oxides, which were synthesized by a modified citrate acid process, was investigated in detail. The chelate processes in precursors with pH values of 1 and 3 were obviously different from those with pH values of 5, 7, and 9. Compared with the samples (pH = 5, 7, and 9), the powders and membranes derived from the precursors with lower pH values (pH = 1 and 3) exhibited different sinterability, crystal development, and morphologies. Due to the differences in membrane microstructures, the LSCF membranes originating from the precursors with lower pH values (pH = 1 and 3) exhibited much larger apparent activation energy for oxygen permeation than the other samples (pH = 5, 7, and 9) in the range of 1073-1123K. Our study demonstrates that the material properties of perovskite-type oxides can be tailored by controlling the pH values in the synthesis process.

Acknowledgments

This work is sponsored by the National Basic Research Program of China (No. 2003CB615702), National Natural Science Foundation of China (NNSFC, No. 20125618), Scientific Research Foundation for the Returned Overseas China Scholars, State Education Ministry (2004527), and the Key Laboratory of Material-oriented Chemical Engineering of Jiangsu Province.

Literature Cited

1. Bouwmeester HJM, Burggraaf AJ. *Fundamentals of Inorganic Membrane Science and Technology.* Amsterdam: Elsevier; 1996.
2. Karton VV, Naumovich EN, Nikolaev AV. Materials of high-temperature electrochemical oxygen membranes. *J Membr Sci.* 199;111:149-157.
3. Stevenson JW, Armstrong TR, Carmeim RD, Pederson JR, Weber WJ. Electrochemical properties of mixed conducting perovskites $La_{1-x}M_xCo_{1-y}Fe_yO_{3-\delta}$ (M = Sr, Ba, Ca). *J Electrochem Soc.* 1996; 143:2722-2729.
4. Balachandran U, Ma B, Maiya PS, Mieville RL, Dusek JT, Picciolo JJ, Guan J, Dorris SE, Liu M. Development of mixed-conducting oxides for gas separation. *Solid State Ionics.* 1998;108:363-370.
5. Tsai C-Y, Dixon AG, Ma YH, Moser WR, Pascucci MR. Dense perovskite, $La_{1-x}A_xFe_{1-y}Co_yO_{3-\delta}$ (A= Ba, Sr, Ca), membrane synthesis, applications and characterization. *J Am Ceram Soc.* 1998;81:1437-1444.
6. Wang HH, Yang WS, Cong Y, Zhu XF, Lin YS. Structure and oxygen permeability of a dual-phase membrane. *J Membrane Sci.* 2003;224: 107-115.
7. Figueiredo FM, Karton VV, Viskup AP, Frade JR. Surface enhanced oxygen permeation in $CaTi_{1-x}Fe_xO_{3-\delta}$ ceramic membranes. *J Membrane Sci.* 2004;236:73-80.
8. Yasumoto K, Inagaki Y, Shiono M, Dokiya M. An (La,Sr)(Ca,Cu)$O_{3-\delta}$ cathode for reduced temperature SOFCS. *Solid state Ionics.* 2002;148: 545-549.
9. Hart NT, Brandon NP, Day MJ, Lapena-Rey N. Functionally graded composite cathode for solid oxide fuel cells. *J Power Sources.* 2002; 106:42-50.
10. Simner SP, Shelton JP, Anderson MD, Stevenson JW. Interaction between La(Sr)FeO_3 SOFC cathode and YSZ electrolyte. *Solid State Ionics.* 2003;161:11-18.
11. Shao ZP, Haile SM. A high-performance cathode for the next generation of solid-oxide fuel cells. *NATURE.* 2004;431:170-173.
12. Balachandran U, Dusek JT, Sweeney SM, Mieville RL, Poppel RB, Kleefisch MS, Pei S, Kobylinski TP, Udovich CA, Bose AC. Dense ceramic membranes for partial oxidation of methane to syngas. *Appl Catal A.* 1995;133:19-29.
13. Jin WQ, Li SG, Huang P, Xu N. P, Shi J. Tubular lanthanum cobaltite perovskite-type membrane reactors for partial oxidation of methane to syngas. *J Membrane Sci.* 2000;166:13-22.
14. Gu XH, Jin WQ, Chen CL, Xu NP, Shi J. YSZ-$SrCo_{0.4}Fe_{0.6}O_{3-\delta}$ membranes for the partial oxidation of methane to syngas. *AICHE J.* 2002;48(9):2051-2060.
15. Gu XH, Yang L, Tan L, Jin WQ, Zhang LX, Xu NP. Modified operating mode for improving the lifetime of mixed-conducting ceramic membrane reactors in the POM environment. *Ind Eng Chem Res.* 2003;42:795-801.
16. Chen CS, Feng SJ, Ran S, Zhu DC, Liu W, Bouwmeester HJM. Conversion of methane to syngas by a membrane-based oxidation-reforming process. *Angew Chem Int Ed.* 2003;42:5196-5198.
17. Fan YQ, Ren JY, Onstot W, Pasale J, Tsotsis TT. Reactor and technical feasibility aspects of a CO_2 decomposition-based power generation cycle, utilizing a high-temperature membrane reactor. *Ind Eng Chem Res.* 2003;42:2618-2626.
18. Zhang P, Chang XF, Wu ZT, Jin WQ, Xu NP. Effect of the packing amount of catalysts on the partial oxidation of methane reaction in a dense oxygen-permeable membrane reactor. *Ind Eng Chem Res.* 2005; 44:1954-1959.
19. Kharton VV, Yaremchenko AA, Tsipis EV, Valente AA, Patrakeev MV, Shaula AL, Frade JR, Rocha J. Characterization of mixed-conducting $La_2Ni_{0.9}Co_{0.1}O_{4+\delta}$ membranes for dry methane oxidation. *Appl Catal A.* 2004;261:25-35.
20. Zeng Y, Lin YS, Swartz SL. Perovskite-type ceramic membrane: synthesis, oxygen permeation and membrane reactor performance for oxidative coupling of methane. *J Membr Sci.* 1998;150:87-98.
21. Li SG, Jin WQ, Xu NP, Shi J. Synthesis and oxygen permeation

properties of $La_{0.2}Sr_{0.8}Co_{0.2}Fe_{0.8}O_{3-\delta}$ membranes. *Solid State Ionics.* 1999;124:161-170.
22. Jin WQ, Abothu IR, Wang R, Chung TS. Sol-gel synthesis and characterization of $SrFeCo_{0.5}O_{3.25-\delta}$ powder. *Ind Eng Chem Res.* 2002; 41:5432-5435.
23. Tan L, Gu XH, Yang L, Jin WQ, Zhang LX, Xu NP. Influence of powder synthesis methods on microstructure and oxygen permeation performance of $Ba_{0.5}Sr_{0.5}Co_{0.8}Fe_{0.2}O_{3-\delta}$ perovskite-type membranes. *J Membrane Sci.* 2003;212:157-165.
24. Deng ZQ, Liu W, Peng DK, Chen CS, Yang WS. Combustion synthesis, annealing, and oxygen permeation properties of $SrFeCo_{0.5}O_y$ membranes. *Mater Res Bull.* 2004;39:963-969.
25. Wang HT, Liu XQ, Zheng H, Zheng WJ, Meng GY. Gel-casting of $La_{0.6}Sr_{0.4}Co_{0.8}Fe_{0.2}O_{3-\delta}$ from oxide and carbonate powders. *Ceram Int.* 1999;25:177-181.
26. Mori M, Sammes NM, Tompsett GA. Fabrication processing condition for dense sintered $La_{0.6}AE_{0.4}MnO_3$ perovskite synthesized by the coprecipitation method (AE=Ca and Sr). *J Power Sources.* 2000;96: 395-400.
27. Aboth IR, Jin W, Wang R, Chung T-S. Effect of hydrolysis rates on the morphology of sol-gel derived $SrFeCo_{0.5}O_x$ powder. *J Mater Sci.* 2004;39:707-709.
28. Li SG, Qi H, Xu NP, Shi J. Tubular dense perovskite type membrane, preparing, sealing, and oxygen permeation properties. *Ind Eng Chem Res.* 1999;38:5028-5033.
29. Alejandro S, Mavis LM, Gilberto M, Ventura T-L, Victor MC. Effect of pH on the precipitation of hydroxyapatite on silica gels. *Mat Res Innovat.* 2003;7:68-73.
30. Xie D, Pan W. Study on $BaBi_4Ti_4O_{15}$ nanoscaled powders prepared by sol-gel method. *Materials Letters* 2003;57:2970-2974.
31. Blank DHA, Kruidhof H, Flokstra J. Preparation of $YBa_2Cu_3O_{7-\delta}$ by citrate synthesis and pyrolysis. *J Phys D: Appl Phys.* 1988;21:226-227.
32. Pechini MP. U.S. Patent No. 3 330 697; 1967.
33. Martell AE, Smith RM. *Critical Stability Constants.* Vol. 3. New York: Plenum Press; 1977.
34. Fan C-L, Ciardullo D, Huebner W. Synthesis of modified $PbTiO_3$ powders and fibers by a liquid mix process. *Mater Sci Eng.* 2003; B100:1.
35. Liu ML, Wang DS. Preparation of $La_{1-z}Sr_zCo_{1-y}Fe_yO_{3-x}$ thin flims, membranes, and coating on dense and porous substrates. *Mater Res Soc.* 1995;10:3210-3221.
36. Teraoka Y, Nobunaga T, Yamazoe N. Effect of cation substitution on the oxygen semipermeability of perovskite oxides. *Chem Lett.* 1988; 503-506.
37. Li SG, Jin WQ, Huang P, Xu NP, Shi J. Comparison of oxygen permeability and stability of perovskite type $La_{0.2}A_{0.8}Co_{0.2}Fe_{0.8}O_{3-\delta}$ (A = Sr, Ba, Ca) membranes. *Ind Eng Chem Res.* 1999;38:2963-2972.
38. Li SG, Jin WQ, Huang P, Xu NP, Shi J. Perovskite-related ZrO_2-doped $SrCo_{0.4}Fe_{0.6}O_{3-\delta}$ membrane for oxygen permeation. *AICHE J.* 1999; 45:276-284.
39. Matzapetakis M, Raptopoulou CP, Tsohos A, Papefthymiou B, Moon N, Salifoglou A. Synthesis, spectroscopic and structural characterization of the first mononuclear, water soluble iron-citrate complex, $(NH_4)_5Fe(C_6H_4O_7)_2 \cdot 2H_2O$. *J Am Chem Soc.* 1998;120:13266-13267.
40. Matzapetakis M, Raptopoulou CP, Terzis A, Lakatos A, Kiss T, Salifoglou A. Synthesis, structure characterization, and solution behavior of the first mononuclear, aqueous aluminum citrate complex. *Inorg Chem.* 1999;38:618-619.
41. Dakanali M, Kefalas ET, Raptopoulou CP, Terzis A, Mavromoustakos T, Salifglou A. Synthesis and spectroscopic and structural studies of a new cadmium (ii)-citrate aqueous complex. Potential relevance to cadmium (II)-citrate speciation and links to cadmium toxicity. *Inorg Chem.* 2003;42:2531-2537.
42. Sammells AF, Cook RL, White JH, Osborne JJ, Macduff RC. Rational selection of advanced solid electrolytes for intermediate temperature fuel. *Solid State Ionics.* 1992;52:111-123.

Manuscript received Apr. 3, 2005, and revision received July 11, 2005.